Guiding light via geometric phases

Sergei Slussarenko,[1,2] Alessandro Alberucci,[3,4] Chandroth P. Jisha,[5] Bruno Piccirillo,[1] Enrico Santamato,[1] Gaetano Assanto,[3,4] and Lorenzo Marrucci[1,6]

[1] *Dipartimento di Fisica, Università di Napoli Federico II, Complesso Universitario di Monte S. Angelo, via Cintia, 80126 Napoli, Italy*

[2] *Centre for Quantum Dynamics and Centre for Quantum Computation and Communication Technology, Griffith University, Brisbane, Queensland 4111, Australia*

[3] *Nonlinear Optics and OptoElectronics Lab, University Roma Tre, I-00146 Rome, Italy*

[4] *Optics Lab, Department of Physics, Tampere University of Technology, FI-33101 Tampere, Finland*

[5] *Centro de Física do Porto, Faculdade de Ciências, Universidade do Porto, 4169-007 Porto, Portugal*

[6] *Consiglio Nazionale delle Ricerche, Institute of Applied Science & Intelligent Systems (ISASI), Via Campi Flegrei 34, 80078 Pozzuoli (NA), Italy*

(Dated: March 22, 2016)

Abstract

All known methods for transverse confinement and guidance of light rely on changes of the refractive index, that is, on scalar properties of electromagnetic radiation[1–11]. Here we disclose a novel concept of dielectric waveguide, exploiting vectorial spin-orbit interactions of light and the resulting geometric phases[12–17]. It relies on anisotropic media whose optic axis lies orthogonal to the propagation direction and is spatially modulated, so that refractive indices remain constant everywhere, yet a spin-controlled cumulative phase distortion is imposed on the beam, balancing diffraction for a specific polarization. Besides theoretical analysis and numerical simulations, we present a proof-of-principle experimental demonstration of a geometric-phase optical waveguide based on a discrete-element implementation. Our findings show that geometric phases may determine the optical behavior in three-dimensional structured media extending well beyond a Rayleigh length, paving the way to a new class of photonic devices. Analogous results apply to the whole electromagnetic spectrum.

Waveguides are central to modern photonics and optical communications. Besides the standard optical fibers –based on total internal reflection (TIR) and graded-index (GRIN) refractive potential– and the hollow-metal-pipes for microwaves[1], several more complex structures have been investigated, ranging from photonic-bandgap systems[2–5] to "slot" waveguides[6], plasmonic waveguides[7], coupled-resonators[8,9], grating-mediated[10] and Kapitza-effect waveguides[11]. Despite such variety, all light-guiding mechanisms investigated hitherto rely on variations, sudden or gradual, of the refractive index or -generally- the dielectric permittivity. Even when anisotropic materials are employed to realize waveguides, as for example in liquid crystals[18], light confinement is based on the transverse modulation of the refractive index experienced by extraordinary waves through the nonuniform orientation of the optic axis with respect to the wave-vector. A fundamental question is whether the guided propagation of light can be achieved at all in structures without perturbations of the refractive index. As we shall prove, this is indeed possible provided that the transverse trapping is purely based on vectorial effects, that is, it relies on spin-orbit interactions between wave propagation and polarization states of light[12,13]: otherwise stated, an entirely new mechanism for light confinement.

Spin-orbit photonic interactions are strictly related to geometric Berry phases[14–17]. In the context of optics, the latter are phase retardations linked exclusively to the geometry of the transformations imposed to light by the medium and independent of the optical path length[12]. This concept has been already implemented in optical elements with various architectures, including patterned dielectric gratings, liquid crystals and metasurfaces[19–23]. These devices exploit the medium anisotropy to modulate the polarization state of light in a space-varying manner across the plane transverse to propagation. This, in turn, gives rise to a spatially inhomogeneous Pancharatnam-Berry (PB) phase[16,24], resulting in a reshaped optical wavefront. Hence, a PB optical element (PBOE) behaves as a phase mask, despite exhibiting constant ordinary and extraordinary refractive indices and a transversely-uniform optical path length, that is a flat geometry. The PB geometric phase should not be confused with the Rytov-Vladimirskii-Berry geometric phase, or "spin-redirection" phase, which can also affect light propagation by inducing an additional spin-dependent spatial shift in optical media that present a transverse gradient of (isotropic) dielectric permittivity, and which is at the core of the optical Magnus effect and the spin Hall effect of light[25,26].

In this work we disclose the possibility of transversely confining electromagnetic waves

(and in particular light), as in a waveguide, by exploiting PB phases to continuously compensate diffraction in a bulk, that is in an extended continuous medium supporting beam propagation over several Rayleigh distances. As we will show, at variance with PBOEs this requires birefringent materials whose optic axis is modulated both in the transverse plane and in the longitudinal coordinate along the propagation direction, a medium structured in three-dimensions (3D).

We investigate light propagation along the axis z of an inhomogeneous uniaxial dielectric. The optic axis $\hat{u}$ is assumed to be space-varying, but lying everywhere in the xy plane transverse to propagation. Its point-wise orientation is described by the angle $\theta(x, y, z)$ between $\hat{u}$ and the y axis in the laboratory frame (see Fig. 1**a**). We also assume that the principal values $\epsilon_{\parallel}$ and $\epsilon_{\perp}$ of the (relative) permittivity tensor are uniform, corresponding to constant refractive indices $n_o = \sqrt{\epsilon_{\perp}}$ and $n_e = \sqrt{\epsilon_{\parallel}}$ for ordinary and extraordinary eigenwaves, respectively.

Let us first recall that, in a homogeneous uniaxial with plane waves propagating with wave-vector along z, the ordinary and extraordinary eigenfields have amplitudes $\psi_o(z) = e^{ik_0 n_o z}\psi_o(0)$ and $\psi_e(z) = e^{ik_0 n_e z}\psi_e(0)$, respectively, with $k_0 = 2\pi/\lambda$ the vacuum wavenumber and λ the wavelength. In other words, the two waves propagate independently of each other and acquire a relative phase retardation $\delta(z) = k_0 \Delta n z$ versus propagation, where $\Delta n = n_e - n_o$ is the birefringence. Without loss of generality, we consider a positive uniaxial medium, that is $\Delta n > 0$. If we now turn from the usual ordinary/extraordinary linear polarization basis to the left/right (L/R) circular polarization (CP) basis, the same evolution for LCP/RCP wave amplitudes is described by (see Methods for a derivation):

$$\begin{aligned}
\psi_L(z) &= e^{i\bar{n}k_0 z}\left[\cos\left(\frac{\delta}{2}\right)\psi_L(0) - i\sin\left(\frac{\delta}{2}\right)e^{i2\theta}\psi_R(0)\right] \\
\psi_R(z) &= e^{i\bar{n}k_0 z}\left[\cos\left(\frac{\delta}{2}\right)\psi_R(0) - i\sin\left(\frac{\delta}{2}\right)e^{-i2\theta}\psi_L(0)\right],
\end{aligned} \tag{1}$$

where $\bar{n} = (n_o + n_e)/2$ is the average refractive index. Equations (1) point out that the two forward-propagating circular waves evolve with a common phase $\bar{n}k_0 z$ and, in addition, periodically exchange handedness (that is LCP becomes RCP and vice versa) acquiring an additional phase factor $\pm 2\theta$ ($+/-$ for initial RCP/LCP, respectively). This extra phase clearly has a geometric nature and is an example of PB phase[16,17,24]. It should be also noted that this phase is not arising from modulations of the ordinary and extraordinary refractive

indices, which are constant in the medium, nor with net energy exchanges between the ordinary and extraordinary linearly-polarized wave components, which remain constant in amplitude all along. The two CP waves completely interchange after a propagation distance $z_{\mathrm{coh}}/2$ such that $\delta(z_{\mathrm{coh}}/2) = \pi$, then the process reverts and the optical field retrieves its initial state in $z = z_{\mathrm{coh}}$ where $\delta(z_{\mathrm{coh}}) = 2\pi$ (see Fig. 1**b**). Hence, the geometric phase in such uniform medium oscillates but does not accumulate over distance. While in PBOEs the propagation can be halted when $\delta(z) = \pi$ by properly arranging the medium length (or its birefringence), so as to obtain a non vanishing PB phase at the output, in a system with extended propagation length (e.g. a waveguide) the described geometric phase appears to play no significant role.

A simple equalization approach to build-up a geometric phase along z consists of introducing a periodic modulation in order to counteract its recurring cancellation, analogous to dispersion-compensation in fibers and quasi-phase-matching in nonlinear optics[27,28]. This requires to periodically invert the sign of θ along z with the same spatial period as the "natural" interchange described above, so that the PB phase will keep adding up (with the same positive or negative sign depending on the input polarization) and accumulate monotonically over distance (Fig. 1**b**). That is, we must have $\theta(z) = \theta(z + \Lambda)$ where $\Lambda = z_{\mathrm{coh}} = 2\pi/(\Delta n k_0) = \lambda/\Delta n$ (the average value of $\theta(z)$, even if nonzero, plays no role). The resulting PB phase can then be exploited to control light over an extended propagation length. In particular, to achieve light confinement the phase retardation needs to be larger on the beam axis than in the outer regions, as in TIR or GRIN optical fibers. Such a phase modulation across the beam gives rise to a focusing effect able to counteract the natural diffraction and leading to transverse confinement and guidance. By combining longitudinal (z) and transverse (xy plane) modulations of θ, an overall 3D structure described by $\theta(x, y, z) = \sigma(z)\Gamma(x, y)$ is obtained, with $\sigma(z) = \sigma(z + \Lambda)$ a periodic function to yield a monotonic growth of the geometric phase and $\Gamma(x, y)$ a transverse profile which defines the waveguide cross-section. A sample sketch of such a structure is in Fig. 1**c**, whereas Fig. 1**d** shows the corresponding geometric phase accumulation in the plane-wave limit. We stress that in this inhomogeneous anisotropic medium the optic axis $\hat{u}$ remains always orthogonal to the propagation direction, so no changes to the ordinary or extraordinary refractive indices may contribute to guiding. Moreover, it will be shown that, within the validity domain of our approximations, no energy exchange between ordinary and extraordinary polarization

components takes place, so that no variation of the average refractive index can contribute as well.

We developed a full analytic theory of the afore described PB guiding mechanism in the frame of the slowly-varying-envelope and small-anisotropy approximations (see Methods). The main results, in a simpler geometry with one transverse coordinate x for the sake of simplicity and assuming a sinusoidal z-modulation for θ, can be summarized in a dynamical equation for the wave amplitude A corresponding to a given CP input:

$$i\frac{\partial A}{\partial z} = -\frac{1}{2\bar{n}k_0}\frac{\partial^2 A}{\partial x^2} + V(x)A \tag{2}$$

where $V(x) \approx \pm(\pi/\Lambda)\Gamma(x)$ with $+/-$ for input LCP/RCP, respectively. Higher-order small corrections to $V(x)$ have been omitted for simplicity (see Methods for the complete expression). Equation (2) is fully equivalent to a 1D Schrödinger equation for a particle oscillating in a potential $V(x)$ (with z playing the role of time) or to the standard (paraxial) Helmholtz equation for light propagating in a GRIN medium with refractive index $n(x)$ such that $V(x) = -k_0[n^2(x) - \bar{n}^2]/(2\bar{n})$. Depending on the sign of $\Gamma(x)$, either LCP or RCP perceive a trapping potential and get confined, while the orthogonal CP undergoes defocusing and diffracts even faster than normal, confirming once again the spin-orbit nature of this interaction. For the confined CP component the structure behaves as a standard GRIN waveguide with index profile $n(x)$ (the CP state refers to the input, as the circular polarization continuously evolves between left and right during propagation, see Fig. 2**f**). Examples of the calculated effective potential and corresponding guided modes are given in Fig. 2**a-c**. In order to check the validity of our theory we carried out finite-difference time-domain (FDTD) numerical simulations of light propagation in the waveguide structure, solving the full Maxwell equations in the space-variant birefringent medium. Figure 2**d-f** provides examples of the obtained results, in excellent agreement with the theoretical predictions.

We demonstrated this novel approach to guiding light with a proof-of-principle experiment. Rather than using the continuous structure described above, we realized a simpler "discrete-element" PB-waveguide consisting of equally spaced PBOEs alternating with a homogeneous isotropic dielectric (air); each PBOE is essentially equivalent to a thin slice of the PB-waveguide and acts as a focusing element, that is, a geometric-phase lens (GPL)[17,20,29,30]. In other words, we mimicked the operation of the PB-waveguide with a sequence of equally

spaced converging lenses, exclusively using PB phases (Fig. 3a).

Our GPLs were thin films of a birefringent uniaxial, nematic liquid crystals, having a transverse distribution of the optic axis given by $\theta = \alpha(x^2 + y^2)$, with α a constant, see Fig. 3b. Neglecting diffraction within the finite GPL thickness, the action of each lens on a CP input beam is described by Eqs. (1). For $\delta = \pi$, the polarization handedness is inverted at the output and the outgoing wave acquires a geometric phase $\pm 2\theta(x, y)$, which is equivalent to the phase of a thin lens having focal length $f = \pm\frac{\pi}{2\alpha\lambda}$. Hence, the GPL acts as a focusing element for one CP handedness but defocusing for the opposite one. Since the circular polarization handedness is inverted at each GPL, in order to balance out diffraction throughout the structure, we flipped the sign of α at each step, resulting in a longitudinal θ oscillation as for the continuous PB waveguide case. The fundamental mode of our discrete waveguide, the shape-preserving Gaussian beam that propagates with period equal to the distance d between opposite lenses, has a beam waist $w_0 = \sqrt{\lambda[(4f - d)d]^{1/2}/(2n_i\pi)}$ centered between subsequent GPLs, where n_i is the refractive index of the isotropic medium between elements.

For our experiments, we set up a sequence of five GPLs, rotating every other one by π around the y axis so as to produce alternating signs of α; moreover, exploiting the electro-optic response of nematic liquid crystals, the lenses were electrically tuned to $\delta = \pi$ (see Methods for details). We characterized light propagation in the structure for both LCP and RCP inputs and compared it with free-space propagation. As can be seen in Figs. 3c-e, the experimental results are in very good agreement with the polarization-dependent waveguiding predicted for the continuous case: only one input CP handedness was confined in the PB-waveguide with a shape-preserving mode, whereas the opposite polarization was radiated off almost immediately. The acquired data matched well the theory, as shown in Fig. 3f.

In conclusion, we have shown, both theoretically and experimentally, that geometric Pancharatnam-Berry phases can be used for transverse confinement of electromagnetic waves, thus introducing an entirely new light-guiding principle that exploits spin-orbit optical interactions and the vectorial nature of electromagnetic radiation. Besides its fundamental interest, the proposed approach is technologically relevant for future integrated optics systems, including those involving metasurfaces[22,23]. The development of novel generations of PB guided-wave photonics and manipulation of light is envisioned in dielectrics

and metamaterials for the whole spectrum, from terahertz to ultraviolet.

I. METHODS

A. Dynamics of circularly polarized waves through a uniform uniaxial medium

Plane-wave light propagation along z in a uniform uniaxial medium can be described by a two-component Jones vector $\boldsymbol{\psi}(z)$ (in the bra-ket notation $|\psi\rangle$), representing the complex amplitudes of two orthogonal polarizations which define the chosen basis of the representation. A 2×2 evolution Jones matrix $\boldsymbol{U}(z)$ then links the vector $\boldsymbol{\psi}(0)$ at the input plane $z=0$ with the vector $\boldsymbol{\psi}(z)$ at any given distance z. In the xy laboratory basis, the Jones vector is the same as the (complex) electric field vector $\boldsymbol{\psi}_{xy}=(E_x;E_y)$. A more convenient basis is that of the ordinary/extraordinary linear polarizations, that is $\boldsymbol{\psi}_{oe}=(E_o;E_e)$. These two bases are related by the rotation matrix $\boldsymbol{R}_{xy}(\theta)=(\cos\theta,\sin\theta;-\sin\theta,\cos\theta)$, where θ is the angle formed by the optic axis $\hat{u}$ with the y axis, that is $\boldsymbol{\psi}_{oe}=\boldsymbol{R}_{xy}\cdot\boldsymbol{\psi}_{xy}$. In this oe basis the evolution matrix is diagonal, being given by the following expression:

$$\boldsymbol{U}_{oe}(z)=\begin{pmatrix} e^{ik_0n_oz} & 0 \\ 0 & e^{ik_0n_ez} \end{pmatrix}. \tag{3}$$

Let us now introduce a third convenient basis to represent propagation, that is the LCP/RCP circular polarization basis, hereafter denoted as LR. In this Letter, we adopt the notation $\boldsymbol{\psi}_L=(1;-i)/\sqrt{2}$ (LCP) and $\boldsymbol{\psi}_R=(1;+i)/\sqrt{2}$ (RCP) for the basis unit vectors, corresponding to the source-point-of-view naming convention on CP states. The matrix $\boldsymbol{P}=(1,1;-i,i)/\sqrt{2}$ can then be used to switch the Jones vector from the LR basis to the xy one, while the rotation operator in the LR basis is diagonal and takes the form $\boldsymbol{R}_{LR}(\theta)=(e^{-i\theta},0;0,e^{i\theta})$. The evolution matrix in the LR basis is then given by the following expression:

$$\boldsymbol{U}_{LR}(z;\theta)=\boldsymbol{R}_{LR}^{-1}(\theta)\cdot\boldsymbol{P}^{-1}\cdot\boldsymbol{U}_{oe}(z)\cdot\boldsymbol{P}\cdot\boldsymbol{R}_{LR}(\theta). \tag{4}$$

A straightforward calculation leads from Eq. (4) to Eq. (1). As mentioned in the main text, the resulting polarization dynamics is a periodic oscillation with period $z_{\rm coh}=\lambda/\Delta n$.

Let us consider the solution for a purely circular polarization at the input, e.g. for $\psi_R(0)=$

1 and $\psi_L(0) = 0$. From Eq. (1) we get $\psi_R(z) = e^{i\bar{n}k_0 z}\cos(\frac{\delta}{2})$ and $\psi_L(z) = -ie^{i\bar{n}k_0 z}\sin(\frac{\delta}{2})e^{2i\theta}$. From the latter expression we can calculate the phase difference between two states corresponding to two different orientations for the optic axis, say θ_1 and θ_2, respectively. Following Pancharatnam's original concept[24,31], the phase delay $\Delta\phi(\theta_1, \theta_2)$ is

$$\Delta\phi(\theta_1, \theta_2) = \arg\left[\langle\psi(\theta_1)|\psi(\theta_2)\rangle\right] = \arg\left[\cos^2\left(\frac{\delta}{2}\right) + \sin^2\left(\frac{\delta}{2}\right)e^{2i(\theta_2-\theta_1)}\right]. \tag{5}$$

Expression (5) results in the transverse phase delay plotted in Fig. 1**b** (dashed lines) in the homogeneous limit. When the optic axis distribution is flipped at $\Lambda/2$, the phase delay can be easily obtained from Eq. (4) (solid lines in Fig. 1**b**). When the optic axis distribution is sinusoidally modulated along z, the accumulated $\Delta\phi(\theta_1, \theta_2)$ can be numerically calculated partitioning the medium in several layers, each of them short enough to make the variations of θ negligible within each layer, as shown in Fig. 1**b** (solid lines with circles).

B. Spin-dependent photonic potential

In the paraxial limit (i.e., neglecting the longitudinal field components) and for small birefringence ($\Delta n \ll 1$), the Maxwell equations for the electric field $\boldsymbol{E} = E_x\hat{x} + E_y\hat{y}$ in two dimensions (i.e., with no field evolution across y) can be cast as

$$\frac{\partial^2}{\partial z^2}\begin{pmatrix} E_x \\ E_y \end{pmatrix} = -\frac{\partial^2}{\partial x^2}\begin{pmatrix} E_x \\ E_y \end{pmatrix} - k_0^2\begin{pmatrix} \epsilon_{xx}(x,z) & \epsilon_{xy}(x,z) \\ \epsilon_{yx}(x,z) & \epsilon_{yy}(x,z) \end{pmatrix}\begin{pmatrix} E_x \\ E_y \end{pmatrix}. \tag{6}$$

We wish to adopt now the slowly-varying-envelope approximation (SVEA) (also corresponding to the paraxial wave approximation) so as to obtain a simpler first-order partial differential equation in the evolution coordinate z. SVEA is usually based on the presence of two very different spatial scales for the evolution along z, that is a short scale of order λ and a long scale given by the Rayleigh length $z_R = \pi\bar{n}w^2/\lambda$, where w is the smallest transverse spatial scale of the problem (the beam radius and/or the transverse spatial modulations of the medium). In our case, however, we also have an intermediate scale $\Lambda = z_{\rm coh} = \lambda/\Delta n$, with $\lambda \ll \Lambda \ll z_R$ for reasonable values of Δn and w. It is therefore not convenient to apply the SVEA directly to Eq. (6), as the field components E_x and E_y undergo a relatively rapid evolution on scale Λ because of birefringence. It is more convenient to switch first

to the space-varying *oe* wave basis introduced in Section A, with a rotation by the angle $\theta(x,z)$ around the z axis. This basis change diagonalizes the effect of birefringence and hence allows one to adopt the SVEA in an optimal way, but at the same time it generates the space-varying geometric phases which will affect the resulting slow-envelope dynamics. In the rotated basis, Eq. (6) becomes

$$\frac{\partial^2 \boldsymbol{\psi}_{oe}}{\partial z^2} - 2i\frac{\partial \theta}{\partial z}\boldsymbol{S}_2 \cdot \frac{\partial \boldsymbol{\psi}_{oe}}{\partial z} = -\frac{\partial^2 \boldsymbol{\psi}_{oe}}{\partial x^2} + 2i\frac{\partial \theta}{\partial x}\boldsymbol{S}_2 \cdot \frac{\partial \boldsymbol{\psi}_{oe}}{\partial x} + i\left(\frac{\partial^2 \theta}{\partial x^2} + \frac{\partial^2 \theta}{\partial z^2}\right)\boldsymbol{S}_2 \cdot \boldsymbol{\psi}_{oe} + \left[\left(\frac{\partial \theta}{\partial x}\right)^2 + \left(\frac{\partial \theta}{\partial z}\right)^2\right]\boldsymbol{\psi}_{oe} - k_0^2 \boldsymbol{\epsilon}_D \cdot \boldsymbol{\psi}_{oe}, \tag{7}$$

where we introduced the Pauli matrix $\boldsymbol{S}_2 = (0, -i; i, 0)$ and the diagonalized permittivity tensor $\boldsymbol{\epsilon}_D = (\epsilon_\perp, 0; 0, \epsilon_\parallel)$. We now set $\boldsymbol{\psi}_{oe}(x,z) = \boldsymbol{U}_{oe}(z) \cdot \boldsymbol{\psi}(x,z)$, where $\boldsymbol{U}_{oe}(z)$ is the evolution matrix in the *oe* basis for plane waves in a uniform medium, as given in Eq. (3), and $\boldsymbol{\psi}(z)$ are slowly-varying amplitudes. Moreover, let us assume sinusoidal z-modulation of the optic axis, as given by $\theta(x,z) = \Gamma(x)\sin(2\pi z/\Lambda)$. We now multiply both sides of Eq. (7) by $\boldsymbol{U}_{oe}^{-1}$ from the left and take a z-average over a period Λ of all terms, assuming that the amplitudes $\boldsymbol{\psi}(z)$ vary slow enough that they can be taken out of the averaging operation (this obviously requires $\Lambda \ll z_R$). The quadratic terms in $\theta(x,z)$ will then contribute with a non-vanishing average, independent of the polarization evolution. In addition, the sinusoidal terms linear in $\theta(x,z)$ combine with the oscillations in polarization described by the z-evolved Pauli matrix $\tilde{\boldsymbol{S}}_2(z) = \boldsymbol{U}_{oe}^{-1}(z) \cdot \boldsymbol{S}_2 \cdot \boldsymbol{U}_{oe}(z) = \boldsymbol{S}_2 \cos(k_0 \Delta n z) + \boldsymbol{S}_1 \sin(k_0 \Delta n z)$, where $\boldsymbol{S}_1 = (0, 1; 1, 0)$ is the first Pauli matrix, leading to other phase-matched constant terms. We thus obtain the following dynamical equation for the slow amplitudes $\boldsymbol{\psi}(z)$:

$$\frac{\partial^2 \boldsymbol{\psi}}{\partial z^2} + \left(2ik_0 \boldsymbol{N} - i\frac{2\pi}{\Lambda}\Gamma(x)\boldsymbol{S}_2\right) \cdot \frac{\partial \boldsymbol{\psi}}{\partial z} = -\frac{\partial^2 \boldsymbol{\psi}}{\partial x^2} - 2k_0\frac{\pi}{\Lambda}\Gamma(x)\boldsymbol{S}_2 \cdot \boldsymbol{N} \cdot \boldsymbol{\psi} + i\frac{\partial \Gamma}{\partial x}\boldsymbol{S}_1 \cdot \frac{\partial \boldsymbol{\psi}}{\partial x} + \frac{i}{2}\left[\frac{\partial^2 \Gamma}{\partial x^2} - \left(\frac{2\pi}{\Lambda}\right)^2 \Gamma(x)\right]\boldsymbol{S}_1 \cdot \boldsymbol{\psi} + \frac{1}{2}\left[\left(\frac{2\pi}{\Lambda}\right)^2 \Gamma^2(x) + \left(\frac{\partial \Gamma}{\partial x}\right)^2\right]\boldsymbol{\psi}, \tag{8}$$

in which we introduced the refractive index matrix $\boldsymbol{N} = \sqrt{\boldsymbol{\epsilon}_D} = (n_o, 0; 0, n_e)$. We now divide all terms in Eq. (8) by $2\bar{n}k_0$ and take the two formal limits $\lambda/z_R \to 0$ (SVEA) and $\lambda/\Lambda = \Delta n \to 0$ (small anisotropy approximation), while keeping Λ and z_R to finite values (this step and the subsequent analyses of the relative magnitude of various terms are best done after switching to dimensionless coordinates x/w and z/z_R, but for the sake of brevity

we keep here the dimensional ones). We thus obtain

$$i\frac{\partial \boldsymbol{\psi}}{\partial z}= -\frac{1}{2\bar{n}k_0}\frac{\partial^2 \boldsymbol{\psi}}{\partial x^2} - \frac{\pi}{\Lambda}\Gamma(x)\boldsymbol{S}_2\cdot\boldsymbol{\psi} + \frac{i}{2\bar{n}k_0}\frac{\partial \Gamma}{\partial x}\boldsymbol{S}_1\cdot\frac{\partial \boldsymbol{\psi}}{\partial x} + \frac{i}{4\bar{n}k_0}\left[\frac{\partial^2\Gamma}{\partial x^2} - \left(\frac{2\pi}{\Lambda}\right)^2\Gamma(x)\right]\boldsymbol{S}_1\cdot\boldsymbol{\psi}$$
$$+\frac{1}{4\bar{n}k_0}\left[\left(\frac{2\pi}{\Lambda}\right)^2\Gamma^2(x) + \left(\frac{\partial\Gamma}{\partial x}\right)^2\right]\boldsymbol{\psi}. \tag{9}$$

Analyzing the magnitude of the four terms containing the optic axis perturbation $\Gamma(x)$, we can see that the last three are of order Λ/z_R relative to the first. Hence, as a zero-order approximation in Λ/z_R we can drop the last three terms, obtaining

$$i\frac{\partial \boldsymbol{\psi}}{\partial z} = -\frac{1}{2\bar{n}k_0}\frac{\partial^2 \boldsymbol{\psi}}{\partial x^2} - \frac{\pi}{\Lambda}\Gamma(x)\boldsymbol{S}_2\cdot\boldsymbol{\psi}. \tag{10}$$

In this equation the only nondiagonal matrix is $\boldsymbol{S}_2$. Its eigenvectors are obviously the circular polarizations $\boldsymbol{\psi}_R$ and $\boldsymbol{\psi}_L$ (with reference to the input plane), with eigenvalues $s_z = \pm 1$, corresponding to the photon spin along z (in $\hbar$ units). Hence, setting $\boldsymbol{\psi}(x,z) = \boldsymbol{\psi}_P A(x,z)$, with $P = L$ or $P = R$ for the two circular-polarized input waves, we obtain the following final amplitude propagation equation:

$$i\frac{\partial A}{\partial z} = -\frac{1}{2\bar{n}k_0}\frac{\partial^2 A}{\partial x^2} - s_z\frac{\pi}{\Lambda}\Gamma(x)A, \tag{11}$$

where $s_z = +1$ for input RCP and $s_z = -1$ for input LCP.

We can then reconsider perturbatively the contribution of the three omitted terms in $\Gamma(x)$ which we had previously dropped. The second and third terms, which are linear in $\Gamma(x)$, include the matrix $\boldsymbol{S}_1$ which flips the CP handedness. Hence these two terms are off-diagonal in the CP basis. The term which is quadratic in $\Gamma(x)$ is instead scalar and hence is diagonal in the CP basis (and in any other basis). Hence, the latter is the only relevant contribution to first order in Λ/z_R, while the other two will contribute to the eigenvalues only to order $(\Lambda/z_R)^2$. In conclusion, up to first order in Λ/z_R we can consider the following final expression for the photonic potential

$$V(x) = -s_z\frac{\pi}{\Lambda}\Gamma(x) + \frac{1}{4\bar{n}k_0}\left[\left(\frac{2\pi}{\Lambda}\right)^2\Gamma^2(x) + \left(\frac{\partial\Gamma}{\partial x}\right)^2\right]. \tag{12}$$

The guided modes of the system can then be obtained by setting $A(x,z) = e^{i\beta z}A(x,0)$, with the effective propagation constant β acting as an eigenvalue. The complete vector expression of the field in the *oe* basis is given by $\boldsymbol{\psi}_{oe}(x,z) = \boldsymbol{U}_{oe}(z) \cdot \boldsymbol{\psi}_P A(x,z)$ with $P = L$ or $P = R$. To obtain the fields in the fixed xy basis one needs to apply also the rotation matrix $\boldsymbol{R}_{xy}^{-1}(x,z)$. It should be noted that, when applied to a single input CP guided mode, this predicted evolution will keep the relative amplitudes of the ordinary and extraordinary waves constantly balanced everywhere in the medium. This justifies our statement that the average refractive index is unperturbed, so that only geometrical phases contribute to the wave confinement.

In the Supplementary Material a more formal theory based on the Bloch-Floquet method is considered in order to analyze the possible additional effects we have neglected in the z-averaging operation. To first order in Λ/z_R, this more complete analysis returns the same results reported here. The quadratic contribution in Γ appearing in Eq. (12) can be neglected for maximum Γ values, that is Γ_0, up to 360° when the transverse size $w \approx 5$ μm, as apparent in Fig. 2**a-b**. This term however becomes relevant for narrower distributions of θ (Supplementary Fig. 1 shows how the trapping potential gets strongly distorted for $\Gamma_0 = 360°$ when $w_D = 0.5$ μm). Finally, the possible long-term role of the higher-order contributions in Λ/z_R, neglected here, will be investigated in future work.

C. FDTD simulations

For the FDTD numerical simulations we employed the open-source code MEEP[32] to solve the full Maxwell equations in two dimensions, with no approximations. In all simulations we assumed a Gaussian shaped orientation of the optic axis across x in the form $\Gamma(x) = \Gamma_0 \exp(-x^2/w_D^2)$. The excitation was a continuous-wave source launched in $x = z = 0$ with a width of 3 μm across x, turned on at $t = 0$ and infinitely narrow across z. The modulated uniaxial medium was placed in $z_0 = 2$ μm with modulation $\sigma(z) = \sin\left[\frac{2\pi\Delta n}{\lambda}(z - z_0)\right]$. The refractive indices n_o and n_e were taken equal to 1.5 and 1.7, respectively. The simulations confirm that an input RCP is confined in the anisotropic structure, whereas an LCP input is expelled towards the edges (Supplementary Fig. 3). The polarization of the simulated confined wave undergoes small variations in the transverse plane (Supplementary Fig. 2) and is not perfectly periodic along z. Such small discrepancies between simulations and

our analytic theory are clearly due to higher-order terms in λ/Λ and Λ/z_R which have been neglected in the analytic theory. For $w_D = 5$ μm light confinement improves with the maximum rotation Γ_0 (Supplementary Fig. 3); however, for $\Gamma_0 = 90°$ even in the defocusing case a small amount of power is trapped on axis owing to the higher order terms appearing in Eq. (12). Further simulations show how light trapping/repulsion both increase as the width w_D gets smaller, in agreement with theory (Supplementary Fig. 5). We also studied numerically the effects of shifting $\sigma(z)$ by changing z_0, obtaining a perfect agreement with theory. In fact, when $z_0 = z_{\rm coh}/2$ the two polarization states exchange their roles, that is, LCP at the input gets trapped whereas a launched RCP undergoes defocusing (Supplementary Fig. 6); when $z_0 = z_{\rm coh}/4$ the beam evolution does not depend on the input polarization, with power equally shared by confined and radiated modes. These results demonstrate that the PB-phase waveguide infringes translational symmetry along the propagation axis, at variance with standard (TIR or GRIN) waveguides. Finally, we numerically ascertained the role of small mismatches between the modulation period Λ and the length $z_{\rm coh}$, an important issue in actual implementations of the proposed waveguides. Keeping all the parameters fixed except for Λ, the global behavior of the two polarization states, i.e., LCP defocused and RCP guided, is robust against Λ variations up to 50%.

D. Fabrication of the geometric phase lenses

Geometric phase lenses and similar PBOEs can be realized with a variety of techniques and materials[19,21,33–35]. Liquid crystals[33] and liquid crystal polymers[34] are the most suitable for visible and near infrared illumination. Our GPLs were fabricated using polarization holography in combination with photo-alignment of nematic liquid crystal[36]. Planar cells were realized with two glass substrates held parallel at a separation of 6 μm, previously coated with a convenient photoaligning surfactant[36]. Such substrates were exposed to collimated ultraviolet light with an inhomogeneous distribution of the linear polarization state. The polarization pattern was realized by coaxial superposition of two beams (473 nm diode-pumped solid-state laser) with orthogonal circular polarizations and various phase-front curvatures. The interference of such beams, rather than an intensity modulation, produces a pattern of linear polarizations, with the angle of the polarization plane proportional to the point-wise phase difference between the beams. After exposure of the coated glass slides, ne-

matic liquid crystals (mixture E7 from Merck) were introduced in the cell by capillarity and aligned with a correspondingly inhomogeneous orientation of the optic axis (molecular director). The required half-wave phase retardation of the GPLs was finely adjusted by applying a 10 kHz square-wave electric voltage ($\approx$ 2.5 V peak-peak) as in other liquid-crystal-based PBOEs[37]. Each GPL can also be optically "switched off" by applying the voltage giving full-wave retardation ($\approx$ 4.0 V). Five GPLs were fabricated, with focal lengths 15.17, 15.98, 14.83, 15.17 and 15.69 $\pm\,0.01$ cm, respectively, for light of wavelength 532 nm. The dispersion of the focal length values is due to the imperfect repeatability of the exposure conditions and insufficient stability of the fabrication setup.

E. Beam characterization within the structure

In order to reconstruct the beam parameters inside the GPL structure, the propagating beam at 532 nm was sampled by a CCD camera placed at various propagation distances between the lenses. Moreover, to improve the measurement accuracy of the local beam parameters, additional beam profiles were collected at given distances from each lens. This was accomplished by either switching off the GPLs following the one under measurement or by physically removing the remaining lenses from the sequence. The beam radii $w(z)$ were obtained through Gaussian fits of the acquired profile images and used to reconstruct the modal parameters within and at the output of the waveguide. The obtained radius evolution was then compared with the theoretical predictions from ABCD Gaussian propagation. A more realistic description of the beam was obtained with a non-unitary beam-quality factor M^2 of the confined beams after each lens ($M_1^2 = 1.05 \pm 0.01$, $M_2^2 = 1.18 \pm 0.02$, $M_3^2 = 1.19 \pm 0.01$, $M_4^2 = 1.15 \pm 0.04$, and $M_5^2 = 1.32 \pm 0.04$, uncertainties at 95% confidence level), suitably modifying the propagation equations[38] for the simulations. The gradual increase of the M^2 parameter after each step of the discrete structure can be ascribed to degradation of the beam profile (as visible in Fig. 3g) due to the noisy patterns of the GPLs.

---

[1] A. W. Snyder and J. D. Love. *Optical Waveguide Theory.* Chapman and Hall, New York, 1983.

[2] P. Yeh and A. Yariv. Bragg reflection waveguides. *Opt. Commun.*, 19:427–430, 1976.

[3] J. D. Joannopoulos, P. R. Villeneuve, and S. H. Fan. Photonic crystals: Putting a new twist on light. *Nature*, 386:143–149, 1997.

[4] J. C. Knight. Photonic crystal fibres. *Nature*, 424:847–851, 2003.

[5] P. Russell. Photonic crystal fibers. *Science*, 299:358–362, 2003.

[6] V. R. Almeida, Q. Xu, C. A. Barrios, and M. Lipson. Guiding and confining light in void nanostructure. *Opt. Lett.*, 29(11):1209–1211, 2004.

[7] J.-C. Weeber, Y. Lacroute, and A. Dereux. Optical near-field distributions of surface plasmon waveguide modes. *Phys. Rev. B*, 68:115401, 2003.

[8] A. Yariv, Y. Xu, R. K. Lee, and A. Scherer. Coupled-resonator optical waveguide: a proposal and analysis. *Opt. Lett.*, 24(11):711–713, 1999.

[9] Q. Lin and S. Fan. Light guiding by effective gauge field for photons. *Phys. Rev. X*, 4:031031, 2014.

[10] O. Cohen, B. Freedman, J. W. Fleischer, M. Segev, and D. N. Christodoulides. Grating-mediated waveguiding. *Phys. Rev. Lett.*, 93:103902, 2004.

[11] A. Alberucci, L. Marrucci, and G. Assanto. Light confinement via periodic modulation of the refractive index. *New J. Phys.*, 15(8):083013, 2013.

[12] K. Y. Bliokh, F. J. Rodriguez-Fortuno, F. Nori, and A. V. Zayats. Spin-orbit interactions of light. *Nature Photon.*, 9:796–808, 2015.

[13] F. Cardano and L. Marrucci. Spin-orbit photonics. *Nature Photon.*, 9:776–778, 2015.

[14] R. Y. Chiao and Yong-Shi Wu. Manifestations of Berry's topological phase for the photon. *Phys. Rev. Lett.*, 57:933, 1986.

[15] F. D. M. Haldane. Path dependence of the geometric rotation of polarization in optical fibers. *Opt. Lett.*, 11:730–732, 1986.

[16] M. V. Berry. The adiabatic phase and Pancharatnam's phase for polarized light. *J. Mod. Opt.*, 34:1401–1407, 1987.

[17] R. Bhandari. Polarization of light and topological phases. *Phys. Rep.*, 281(1):1–64, 1997.

[18] M. Peccianti, C. Conti, G. Assanto, A. De Luca, and C. Umeton. Routing of anisotropic spatial solitons and modulational instability in liquid crystals. *Nature*, 432:733–737, 2004.

[19] Z. Bomzon, V. Kleiner, and E. Hasman. Pancharatnam-Berry phase in space-variant polarization-state manipulations with subwavelength gratings. *Opt. Lett.*, 26(18):1424–1426, 2001.

[20] L. Marrucci, C. Manzo, and D. Paparo. Pancharatnam-Berry phase optical elements for wavefront shaping in the visible domain: switchable helical modes generation. *Appl. Phys. Lett.*, 88:221102, 2006.

[21] S. Slussarenko, A. Murauski, T. Du, V. Chigrinov, L. Marrucci, and E. Santamato. Tunable liquid crystal q-plates with arbitrary topological charge. *Opt. Express*, 19:4085–4090, 2011.

[22] N. Yu and F. Capasso. Flat optics with designer metasurfaces. *Nature Mater.*, 13:139–150, 2014.

[23] D. Lin, P. Fan, E. Hasman, and M. L. Brongersma. Dielectric gradient metasurface optical elements. *Science*, 345:298–302, 2014.

[24] S. Pancharatnam. Generalized theory of interference, and its applications. *Proc. Indian Acad. Sci. A*, 44(5):0370–0089, 1956.

[25] V. S. Liberman and B. Ya. Zel'dovich. Spin-orbit interaction of a photon in an inhomogeneous medium. *Phys. Rev. A*, 46:5199–5207, Oct 1992.

[26] K. Yu. Bliokh and Yu. P. Bliokh. Modified geometrical optics of a smoothly inhomogeneous isotropic medium: The anisotropy, Berry phase, and the optical Magnus effect. *Phys. Rev. E*, 70:026605, Aug 2004.

[27] C. Lin, L. G. Cohen, and H. Kogelnik. Optical-pulse equalization of low-dispersion transmission in single-mode fibers in the 1.3–1.7-μm spectral region. *Opt. Lett.*, 5(11):476–478, 1980.

[28] J. A. Armstrong, N. Bloembergen, J. Ducuing, and P. S. Pershan. Interactions between light waves in a nonlinear dielectric. *Phys. Rev.*, 127:1918–1939, 1962.

[29] E Hasman, V Kleiner, G Biener, and A Niv. Polarization dependent focusing lens by use of quantized Pancharatnam-Berry phase diffractive optics. *Appl. Phys. Lett.*, 82(3):328–330, 2003.

[30] F. S. Roux. Geometric phase lens. *J. Opt. Soc. Am. A*, 23(2):476–482, 2006.

[31] M. V. Berry. Pancharatnam, virtuoso of the Poincaré sphere: an appreciation. *Current Science*, 67:220–223, 1994.

[32] A. F. Oskooi, D. Roundy, M. Ibanescu, P. Bermel, J. D. Joannopoulos, and S. G. Johnson. MEEP: A flexible free-software package for electromagnetic simulations by the FDTD method. *Computer Phys. Commun.*, 181:687–702, 2010.

[33] L. Marrucci, C. Manzo, and D. Paparo. Optical spin-to-orbital angular momentum conversion in inhomogeneous anisotropic media. *Phys. Rev. Lett.*, 96:163905, 2006.

[34] S. Nersisyan, N. Tabiryan, D. M. Steeves, and B. R. Kimball. Fabrication of liquid crystal polymer axial waveplates for UV-IR wavelengths. *Opt. Express*, 17(14):11926–11934, 2009.

[35] C. N. Alexeyev. Circular array of anisotropic fibers: A discrete analog of a q plate. *Phys. Rev. A*, 86:063830, 2012.

[36] V. G. Chigrinov, V. M. Kozenkov, and H.-S. Kwok. *Photoalignment of Liquid Crystalline Materials: Physics and Applications*. Wiley Publishing, 2008.

[37] B. Piccirillo, V. D'Ambrosio, S. Slussarenko, L. Marrucci, and E. Santamato. Photon spin-to-orbital angular momentum conversion via an electrically tunable q-plate. *Appl. Phys. Lett.*, 97(5):241104, 2010.

[38] H. Sun. Thin lens equation for a real laser beam with weak lens aperture truncation. *Opt. Eng.*, 37(11):2906–2913, 1998.

Acknowledgments

The work in Naples was supported by the 7^{th} Framework Programme of the European Commission, within the Future Emerging Technologies program, under grant No. 255914, PHORBITECH, and by the European Research Council (ERC), under grant No. 694683, PHOSPhOR. A.A. and G.A. thank the Academy of Finland for financial support through the FiDiPro grant no. 282858. C.P.J. gratefully acknowledges Fundação para a Ciência e a Tecnologia, POPH-QREN and FSE (FCT, Portugal) for the fellowship SFRH/BPD/77524/2011.

Author Contributions

This work was jointly conceived by A.A., C.P.J., G.A. and L.M.; S.S. designed and carried out the experiment, with the help and supervision of B.P., E.S. and L.M.; A.A. and C.P.J. developed the theory and performed the numerical simulations, with the help and supervision of L.M. and G.A.; all authors discussed the results and contributed to the manuscript.

Additional Information

Supplementary Information is linked to the online version of the paper. Correspondence and requests for materials should be addressed to L.M. or G.A.

Competing financial interests

The authors declare no competing financial interests.

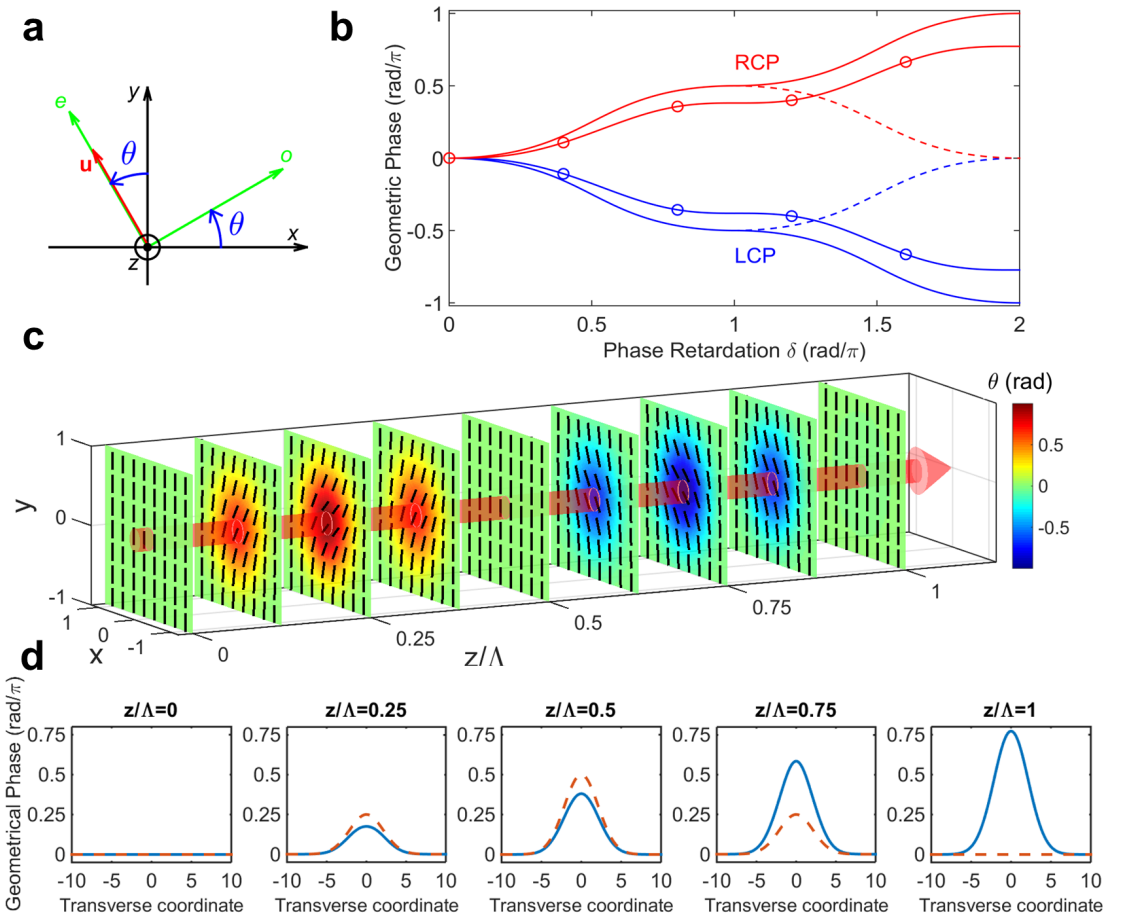

FIG. 1. **Geometric-phase waveguide concept.** **a**, Reference system with orientation of the optic axis $\boldsymbol{u}$ and ordinary/extraordinary (o/e) field directions in the laboratory frame xyz; the angle θ between $\boldsymbol{u}$ and the axis y varies from point to point. **b**, Geometric phase acquired by a plane wave, CP at the input, propagating along z in a transversely homogeneous medium with $\theta = \pi/4$ as a function of the birefringence retardation $\delta(z)$, relative to the case with $\theta = 0$. The geometric phase sign is fixed by the CP input handedness (blue and red lines). If θ is uniform along z (dashed lines), the gometric phase reaches a maximum (in the example $\pi/2$) when $\delta = \pi$ and then decreases to zero for $\delta = 2\pi$. If the angle θ is suddenly inverted at $\delta = \pi$ (solid lines), the phase grows monotonically. If θ is sinusoidally modulated along z (solid lines with circles), the phase increases monotonically at a slightly lower rate than in the previous case. When launching a light beam along z in a periodic uniaxial medium with $|\theta|$ larger on axis than in the outer regions, the cumulative geometric phase leads to a guiding effect for an input LCP or RCP, depending on the initial θ modulation sign. **c**, 3D illustration of a continuously modulated geometric-phase waveguide: the orientation of the optic axis is longitudinally sinusoidal and transversely Gaussian. We sketch nine sections within a modulation period, with the black rods representing the optic axis distribution and the colors corresponding to θ; the guided light beam is represented as a red arrow. **d**, Geometric phase accumulation across the beam profile versus propagation in the plane wave limit (that is, without diffraction), corresponding to **c** (blue solid line) and in the limit of an optic axis that is unmodulated along z (red dashed lines). Here the maximum θ is $\pi/4$.

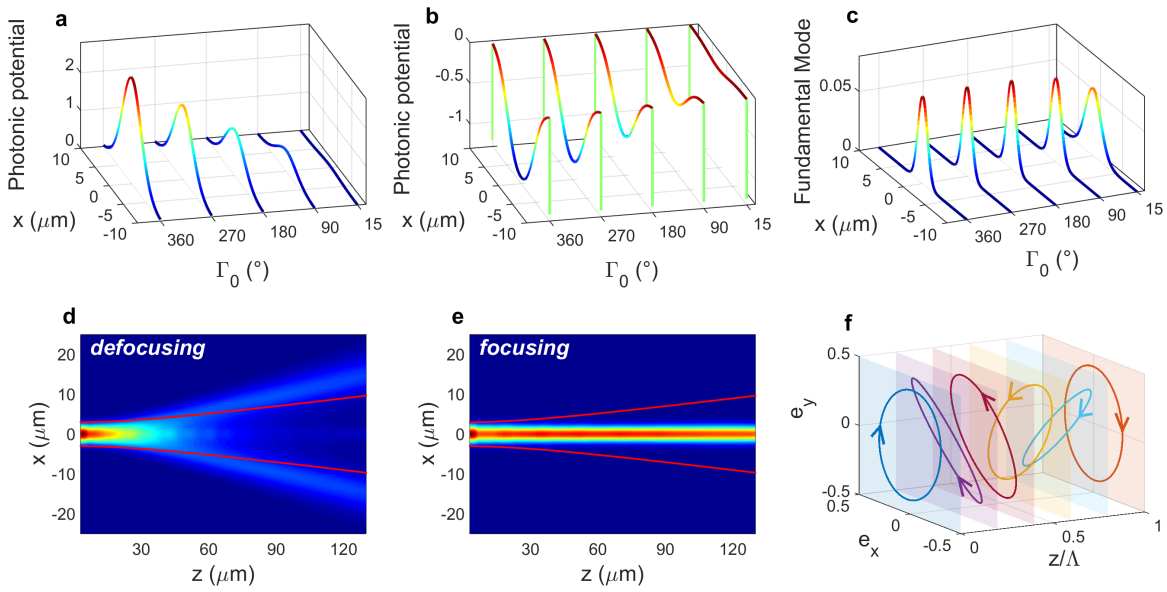

FIG. 2. **Theory and simulations. a-b**, Effective photonic potential $V(x)2\bar{n}/k_0$ versus x and maximum θ angle Γ_0 (we assumed a Gaussian distribution for the transverse orientation by setting $\Gamma = \Gamma_0 \exp(-x^2/w_D^2)$) perceived by the defocused (**a**, LCP input) and the confined (**b**, RCP input) waves, respectively. The terms proportional to Γ^2 are accounted for (see Methods). **c**, Corresponding fundamental guided mode; represented is the field amplitude versus x and Γ_0. **d-f**, FDTD simulations for $\Gamma_0 = 15°$ when the input beam is LCP (**d**) and RCP (**e**), respectively; the color scale gives the local light intensity; the red lines give the beam radius evolution for a homogeneous medium, that is for ordinary diffraction. **f**, Evolution of the confined beam polarization state within a modulation period. Here $\lambda = 1$ μm, $n_o = 1.5$, $n_e = 1.7$, $\sigma(z)$ is sinusoidal and the transverse distribution has $w_D = 5$ μm.

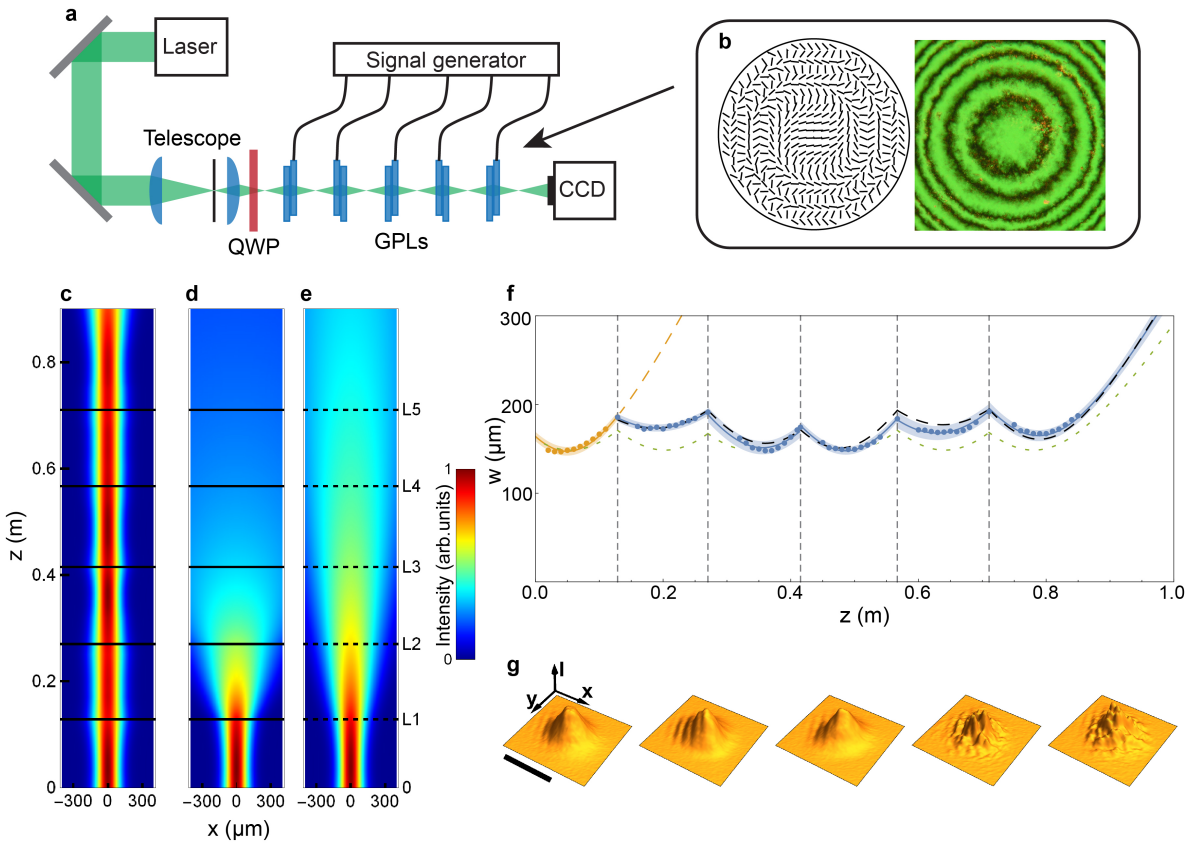

FIG. 3. **Experiment.** **a**, Experimental setup: five equally-spaced electrically-tuned GPLs form a discrete-element geometric-phase waveguide. A 532 nm continuous-wave Gaussian beam was adjusted in transverse size with a telescope so as to match the fundamental mode of the waveguide, circularly polarized with a quarter-wave plate (QWP) and then launched into the waveguide. Beam profiles at various intermediate positions z along the propagation and at the output were acquired by a movable CCD camera and used to reconstruct the mode parameters of the beam after each GPL. **b**, Distribution of the optic axis and corresponding microscope image of a GPL between crossed polarizers; dark fringes correspond to regions where the optic axis is aligned parallel to one of the polarizers. **c**-**e**, Data-reconstructed evolution of the propagating beam for each of the following cases: **c**, guided mode obtained for RCP input; **d**, divergent beam obtained for LCP input; **e**, free-space diffracting beam for the same input parameters. The color scale gives the local light intensity. Horizontal lines and L1-L5 labels indicate the GPL positions within the discrete sequence (dashed lines mark removed GPLs). **f**, Beam radius versus z in the guided case. Dots are the measurement data, the blue solid lines are the Gaussian-beam fits for those dots between two subsequent GPLs, the blue shaded areas being the fit confidence regions at one standard deviation; the black dashed line is the theoretical prediction based on the ABCD method, also accounting for the imperfections of the Gaussian beam (as defined by the M^2 parameter) and of the GPLs; the dashed green line corresponds to the predicted beam evolution for an ideal Gaussian input, with $M^2 = 1$. Vertical dashed lines give the positions of the GPLs in the waveguide. **g**, Acquired intensity beam profiles (I versus x, y) at the input plane of each GPL in the structure for the guided case; the scale-bar corresponds to 400 μm.